Probing Structure and Dynamics in Poly[2,2′-(*m*-phenylene)-5,5′-bibenzimidazole] Fuel Cells with Magic-Angle Spinning NMR

Colan E. Hughes,[†] Stefan Haufe,[‡] Brigitta Angerstein,[†] Ratna Kalim,[‡] Ulrich Mähr,[‡] Annette Reiche,[‡] and Marc Baldus*,[†]

Department of NMR Based Structural Biology, Max Planck Institute for Biophysical Chemistry, Am Fassberg 11, 37077 Göttingen, Germany, and Sartorius AG, August-Spindler-Strasse 11, 37079 Göttingen, Germany

Received: June 3, 2004; In Final Form: July 1, 2004

H_2/air fuel cell polymer electrolyte membranes, consisting of poly[2,2′-(*m*-phenylene)-5,5′-bibenzimidazole] (PBI) doped with phosphoric acid, have been studied by ^{1}H and ^{31}P magic-angle spinning (MAS) NMR to investigate the polymer−acid interaction and the unresolved question of the nature of the proton conductivity. The ^{1}H and ^{31}P resonances have been fully assigned, giving a complete picture of the species present and allowing a study of the local motion of these species by nuclear relaxation. These results have been compared to conductivity measurements, enabling conclusions to be drawn with regard to the molecular motion causing proton conductivity.

Introduction

Understanding the details of proton conduction is important in a variety of chemical processes, from H^+ translocation in membrane proteins to conduction in polymer electrolyte membranes (PEMs). PEMs play a central role in low-temperature (T < 200 °C) fuel cells, conducting protons to facilitate the reaction between a fuel (hydrocarbon, alcohol, or hydrogen) and oxygen (usually in air). One class of PEMs consists of polyprotic acids complexed by a basic polymer, such as poly[2,2′-(*m*-phenylene)-5,5′-bibenzimidazole] (PBI) treated with phosphoric acid.[1] Unlike Nafion-based protonic conductors, PBI + H_3PO_4 electrolytes have high conductivity in the absence of water.[1−9]

Proton hopping (the Grotthuss mechanism)[10,11] and bulk ion transport (Figure 1) have both been proposed as the main source of ion conduction in such proton-conducting polymer membranes,[2−9,12−15] but the details of the conduction mechanism remain elusive.[15] IR spectroscopy has detected H_2PO_{4-} ions for a broad range of doping levels, together with H_3PO_4 molecules at higher doping levels,[5] consistent with an acid-induced protonation of the PBI imidazole nitrogens (Figure 1). However, diphosphate species were not observed and HPO_4^{2-} ions were only observed at low doping levels.

Solid-state nuclear magnetic resonance (SS NMR) is a technique ideally suited to the study of amorphous polymers, as it is able to resolve different chemical environments on the basis of chemical shift dispersion, probe mobility through exchange and relaxation experiments, and identify spatial proximity through correlation experiments.[16] In particular, magic-angle spinning (MAS)[17] NMR has made considerable progress in addressing structural problems involving polymers, biopolymers, and membrane proteins (see, for example, refs 18−20) and has recently been applied to solid oxide fuel cells.[21] In the following, we show how MAS NMR can be used to study acid−polymer interactions and their dynamics at atomic resolution in PBI fuel cells. First, we will use one- and two-dimensional SS NMR experiments to identify and assign the different ^{1}H and ^{31}P environments. Equipped with this information, we will go on to measure the small-scale mobility of the H and P atoms and compare this to the H^+ conductivity for a number of samples of PBI doped with H_3PO_4.

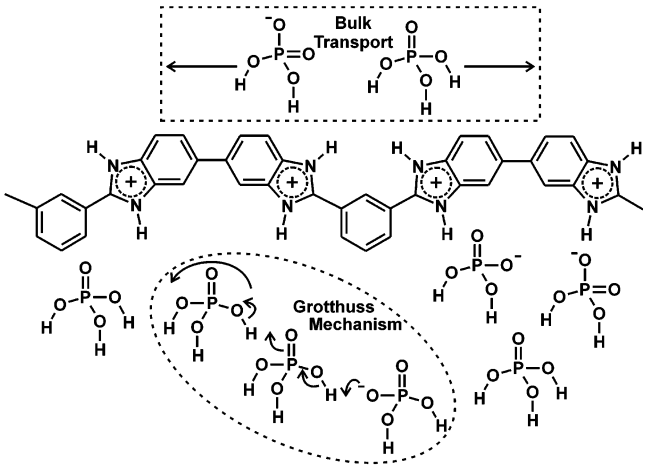

Figure 1. PBI doped with phosphoric acid, showing the result of protonation of the polymer by the acid. Also shown are two possible H^+ conduction mechanisms, Grotthuss and bulk transport.

Experimental Section

Materials and Methods. Samples of PBI + D_3PO_4 were prepared by adding 85% D_3PO_4/D_2O (Aldrich) to dry PBI (Sartorius) in a dry, N_2-purged glass flask. The mixture was dried for 3 h at 100 °C and for 1 h at 160 °C. The sample was stored under exclusion of air. The PBI was characterized by measurement of the intrinsic viscosity of a 1% solution of PBI in dimethylacetamide, which was 0.084 $m^3\ kg^{-1}$. Solvent-free PBI membranes were produced by a pilot plant machine. Four fuel cells (Table 1) were prepared by combining a PBI membrane with single-sided ELAT electrodes (DeNora) im-

* Corresponding author: Tel +49 551 201 2212; fax +49 551 201 2202; e-mail maba@mpibpc.mpg.de.
† Max Planck Institute for Biophysical Chemistry.
‡ Sartorius AG.

10.1021/jp047607c CCC: $27.50
Published on Web 08/17/2004

TABLE 1: Preparation Details for the Four Fuel Cells Studied

fuel cell	wt % H_3PO_4	wt % H_2O	surface area (cm^2)	thickness (μm)
A	70	0	10	41
B	70	5	10	42
C	85	0	10	42
D	85	5	10	41

pregnated with H_3PO_4.[22] All samples were preconditioned for 16 h at 160 °C with N_2 purge. Samples B and D were measured under working conditions, accounting for the 5 wt % water content. Before measurement, sample D was operated as a fuel cell at 160 °C for 20 h. Conductivity measurements were made in a fuel cell under working conditions (samples B and D) or inert conditions (samples A and C) by an IM6 (Zahner Electronics).

For the NMR experiments leading to the ^1H and ^{31}P resonance assignments, deuterated samples were used in order to reduce the otherwise dominant ^1H signal contribution from phosphoric acid. The acidities of D_3PO_4 and H_3PO_4 are very similar (pK_1 of 2.2 and 2.0, respectively),[23] ensuring that the reactivity of the two acids with PBI, and hence the basic structure of the doped samples, will be independent of deuteration. Furthermore, chemical shift changes due to deuteration are in general small and can be neglected in the present study. Because the conductivities of the two acids are substantially different (2.8 S m^{-1} for D_3PO_4 and 4.7 S m^{-1} for H_3PO_4[23]), protonated samples were, however, used for the conductivity measurements and the corresponding line width measurements.

NMR measurements were conducted on 9.4 T (400 MHz ^1H frequency) and 14.1 T (600 MHz ^1H frequency) wide-bore instruments (Bruker Biospin, Germany), employing 2.5 and 4 mm magic-angle spinning probe heads. ^1H and ^{31}P spectra were referenced to 85% H_3PO_4 aqueous solution at 10.5 and 0 ppm, respectively. (^1H,^{31}P) cross polarization (CP)[24] experiments were performed with linear ramps[25] and typical radio frequency (rf) fields of 65 kHz (^1H) and 44 kHz (^{31}P). During ^{31}P acquisition, proton decoupling fields of approximately 65 kHz were employed.

Two different sets of two-dimensional experiments of the general form preparation−(t_1)−evolution−mixing−(t_2) detection were recorded. The (^1H,^{31}P) heteronuclear correlation (HETCOR) experiment[26] consists of an initial time period (t_1) during which ^1H magnetization evolves freely, followed by a CP step that transfers polarization to dipolar-coupled ^{31}P spins, which are detected under ^1H decoupling during t_2. Fourier transformation in both time domains leads to chemical shift correlations of dipolar-coupled (^1H,^{31}P) spin pairs. For the (^1H,^{31}P) HETCOR experiments, 16 transients per t_1 increment and 64 spectra per experiment were accumulated in the two-dimensional data sets. In addition, (^{31}P,^{31}P) exchange spectroscopy (EXSY) experiments[27] were conducted, where evolution (t_1) and detection (t_2) periods record ^{31}P resonances under ^1H decoupling. During mixing, longitudinal (^{31}P,^{31}P) exchange can occur for ^{31}P resonances that either are close in space (spectral spin diffusion) or are undergoing chemical exchange. For the (^{31}P,^{31}P) EXSY experiments, 16 transients per t_1 increment and 128 spectra per experiment were accumulated. Phase-sensitive detection was accomplished by use of time-proportional phase incrementation (TPPI) phase cycling.[27]

Results and Discussion

NMR Experimental Results. Figure 2 shows three one-dimensional spectra of a sample of PBI doped with 69 wt % D_3PO_4. Panel a is from a (^1H,^{31}P) CP experiment while panel b is from a direct 90° pulse excitation experiment. Both were recorded at 100 °C due to the narrower line widths at this temperature. The sample was spun at 6 kHz with ^1H decoupling during acquisition. A one-dimensional ^1H spectrum (direct 90° pulse excitation) is shown in Figure 2c, acquired at low temperature and fast MAS. Doping with D_3PO_4 rather than H_3PO_4 significantly reduces the otherwise dominant ^1H signal of H_3PO_4 (10.5 ppm), which does, however, remain detectable due to ^1H exchange with the polymer. In the (^1H,^{31}P) CP experiment (Figure 2a), polarization transfer is established by through-space dipolar transfer. This experiment therefore examines local acid−polymer interactions. Four resonances (termed P_a−P_d) are observed. The direct 90° pulse excitation experiment (Figure 2b) is sensitive to all ^{31}P nuclei, but this only contains two NMR signals (P_b and P_d). In the ^1H spectrum (Figure 2c), two sharp resonances are found (termed H_c and H_d).

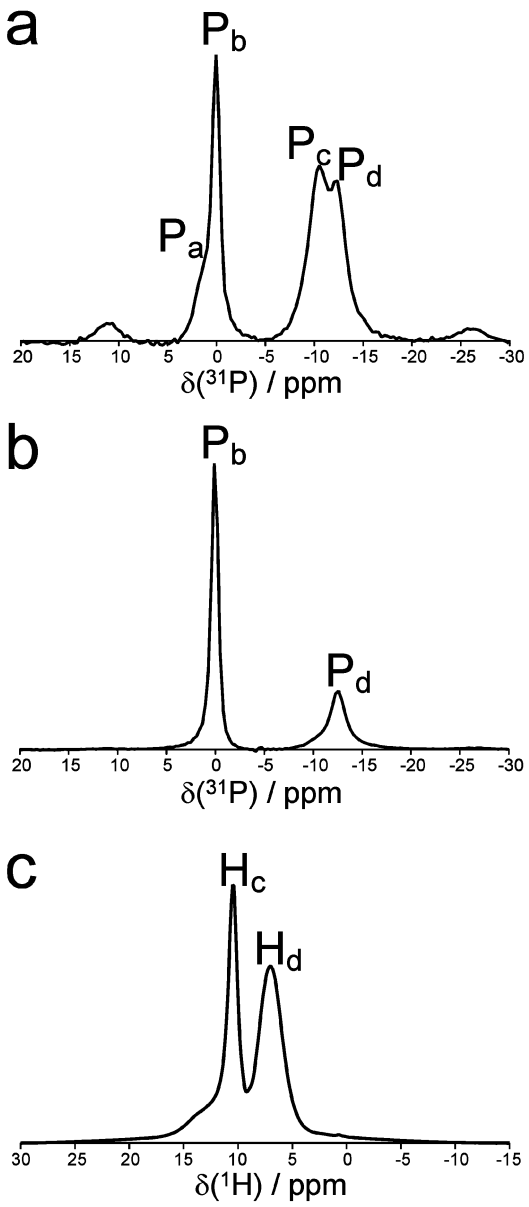

Figure 2. (a) One-dimensional ^{31}P MAS NMR spectra of PBI doped with 69 wt % D_3PO_4 at 100 °C, 14.1 T, and 6 kHz MAS, acquired with 2 ms cross polarization from ^1H nuclei and 65 kHz ^1H decoupling. (b) As in panel a but with direct 90° excitation pulse. (c) One-dimensional ^1H MAS NMR spectrum of PBI doped with 69 wt % D_3PO_4 at −10 °C, 14.1 T, and 22 kHz MAS.

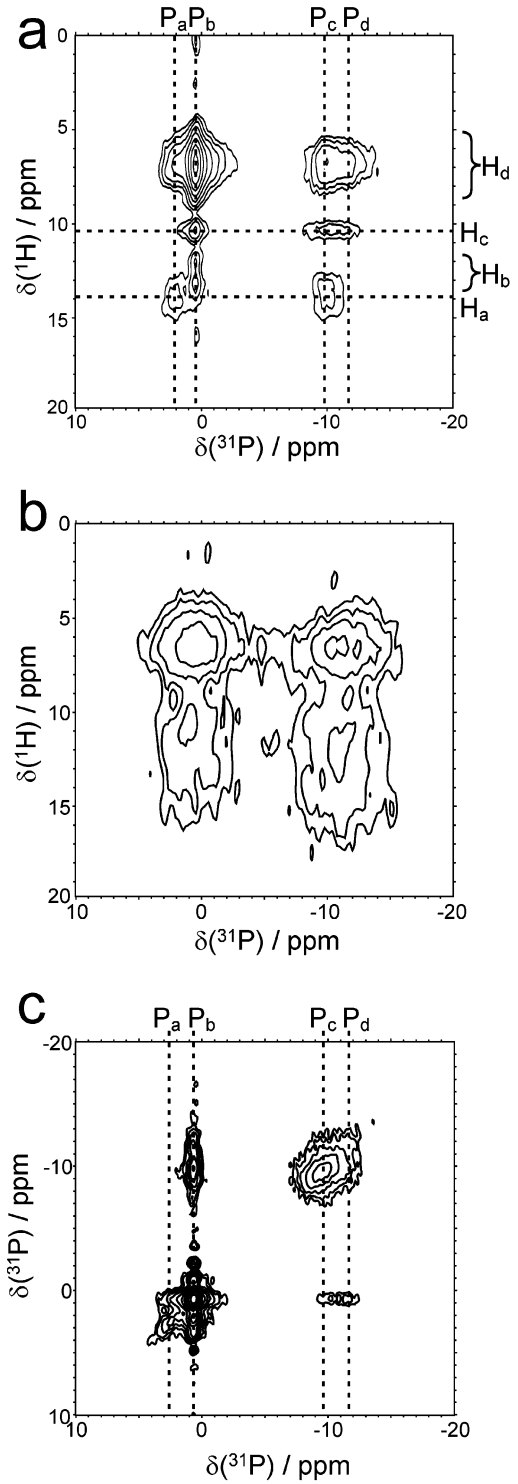

Figure 3. (a) Two-dimensional $^1H-^{31}P$ correlation spectrum of PBI doped with 69 wt % D_3PO_4 at 20°C, 14.1 T, and 22 kHz MAS. Cross polarization of 2 ms was used to transfer magnetization from ^1H to ^{31}P. An additional correlation between P_d and H_b can be seen at lower contour levels. (b) Two-dimensional $^1H-^{31}P$ correlation spectrum of PBI doped with 25 wt % D_3PO_4, same conditions as in panel a. (c) Two-dimensional $^{31}P-^{31}P$ exchange spectrum of PBI doped with 69 wt % D_3PO_4 at 10 °C, 14.1 T, and 22 kHz MAS. An exchange mixing time of 1 s was used.

For a more detailed spectral analysis, we performed a series of ($^1H-^{31}P$) HETCOR experiments. In Figure 3, results obtained on PBI doped with 69 wt % D_3PO_4 (panel a) and with 25 wt % D_3PO_4 (panel b) are shown. The spectral resolution is far better for PBI doped with 69 wt % D_3PO_4, pointing to a high degree of order in this sample, arising from the swelling and partial crystallization of the polymer upon doping. The absence of any broad features in the spectra of the highly doped sample, also observed in the one-dimensional ^{31}P spectra (Figure 2a,b) and ^{13}C spectra (not shown), indicates that all the sample has a similar level of ordering and strongly suggests that this ordering, induced by the phosphoric acid, is occurring throughout the sample. In Figure 3a, the same four ^{31}P resonances are observed as in the one-dimensional spectrum, while two additional ^1H resonances (H_a and H_b) are observed compared to the one-dimensional spectrum in Figure 2c.

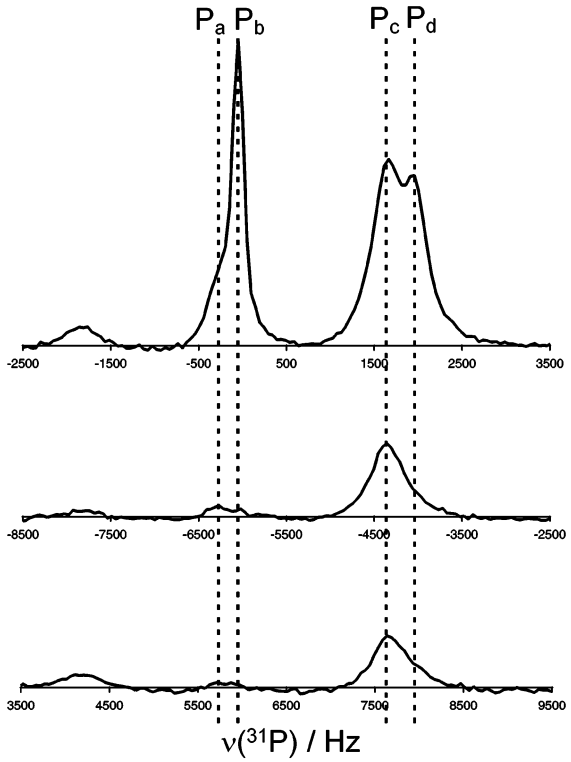

Figure 4. One-dimensional ^{31}P MAS NMR spectrum of PBI doped with 69 wt % D_3PO_4 at 100°C, 14.1 T, and 6 kHz MAS, acquired with 2 ms cross polarization from ^1H nuclei and 65 kHz ^1H decoupling (as in Figure 2a), showing the first-order spinning sidebands below the center band.

To investigate (^{31}P,^{31}P) correlations on the molecular level, we also carried out two-dimensional ($^{31}P-^{31}P$) EXSY exchange experiments with varied mixing times on the sample of PBI doped with 69 wt % D_3PO_4. In Figure 3c, results are shown for a mixing time of 1 s. Exchange between P_a and P_b and between P_c and P_d is seen on a time scale of tens of milliseconds, while slower exchange, on the time scale of hundreds of milliseconds, occurs between P_b and both P_c and P_d. No exchange is seen between P_a and either P_c or P_d.

In addition to the isotropic chemical shift information, the size of anisotropic chemical shielding (CSA) interactions provides a sensitive probe for the electronic environment and molecular mobility and is the dominant interaction for ^{31}P nuclei in phosphate species. Under MAS, CSA interactions lead to the appearance of spinning sidebands. Figure 4 shows the center band of the CP spectrum of PBI doped with 69 wt % D_3PO_4 (as in Figure 2a), with the first-order spinning sidebands below. It can be seen that resonances P_a and P_c have significantly larger spinning sidebands relative to the center bands than P_b and P_d.

Assignment of NMR Spectra. IR spectroscopy indicates that only H_3PO_4 and $H_2PO_4^-$ are present in PBI at high doping levels of phosphoric acid.[5] The chemical shift for phosphoric acid is

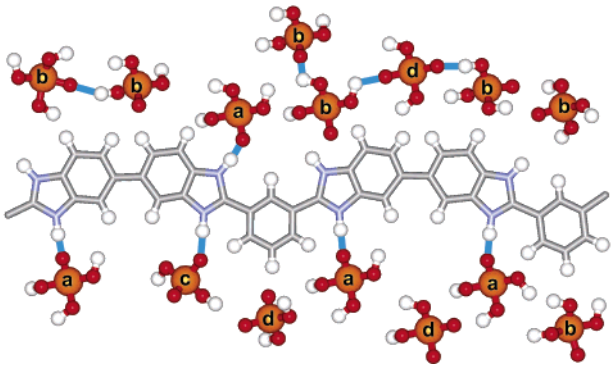

Figure 5. Schematic showing the spectral assignment of PBI doped with phosphoric acid. Blue lines represent hydrogen bonds. Letters correspond to the assignments P_a−P_d. Our results cannot distinguish between imidazoles binding to one or two phosphate species.

0 ppm, and two of the four resonances observed in the ^{31}P spectra have chemical shifts close to 0 ppm, P_a and P_b. We therefore assign these two resonances to H_3PO_4 molecules and attribute the P_c and P_d resonances to $H_2PO_4^-$. These assignments are supported by the observation that exchange is seen on a short time scale between resonances P_a and P_b and between resonances P_c and P_d.

Comparison of the (^1H−^{31}P) CP spectrum (Figure 2a), where all four ^{31}P resonances are observed, and the direct 90° pulse excitation experiment (Figure 2b), where only P_b and P_d are detected, implies that the species P_b and P_d are more abundant than P_a and P_c but reside further from the polymer chain, the main source of ^1H magnetization for CP. All four species must be immobile on the time scale of the MAS rotor period to give significant CP signals. Resonances P_a and P_c have much larger CSAs than P_b and P_d (demonstrated by the larger spinning sidebands, Figure 4). This could imply the presence of two different binding sites or that P_a and P_c are less mobile than P_b and P_d. However, the primary effects on the CSA will come from the immediately bound atoms and the motion of the molecules. Since the local molecular environment (four oxygen atoms) is identical for both considered resonance pairs, we attribute changes in CSA size to increased mobility for the (P_b, P_d) pair relative to (P_a, P_c). In addition, the P_a and P_c resonances are correlated with a ^1H resonance at 14 ppm (H_a), whose chemical shift is strongly indicative of hydrogen-bonded NH.[28] Thus, the resonances P_a and P_c can be assigned to species H-bonded to the polymer through the imidazole NH, while P_b and P_d (which do not correlate to any ^1H resonances at such high chemical shifts) are assigned to species not bound to the polymer.

In addition to the H_a resonance noted above, the narrow H_c resonance may be assigned to free phosphoric acid and ions and the broad H_d resonance to aromatic sites on the polymer. The remaining H_b resonance is only correlated with P_b and P_d (H_b−P_d peak present in the ^1H−^{31}P HETCOR spectrum but below the contours in Figure 3a). The high value of the chemical shift for H_b is suggestive of a hydrogen-bound species, and as it only correlates with free acid and ion ^{31}P sites, H_b is assigned to protons in hydrogen bonds between free acid molecules and/or ions.

The assignment of the ^{31}P and ^1H resonances is shown in Table 2 and is illustrated in Figure 5, showing the four different ^{31}P environments (ions and molecules, bound and unbound). Spectra of samples from fuel cells conform to this assignment.

Comparison of NMR and Conductivity Measurements. The direct-excitation one-dimensional ^{31}P spectrum (Figure 2b) is dominated by P_b and P_d, due to unbound H_3PO_4 and $H_2PO_4^-$, while the main components in the ^1H spectrum (Figure 2c, also direct excitation) are due to unbound $H_3PO_4/H_2PO_4^-$ (H_c) and polymer (H_d) protons. Thus, by monitoring the temperature dependence of the H_c, H_d, and P_b resonances, the dynamics of unbound H_3PO_4 and $H_2PO_4^-$ species may be studied.

TABLE 2: Assignment of ^1H and ^{31}P NMR Resonances

^1H resonances			^{31}P resonances		
	frequency (ppm)	assignment		frequency (ppm)	assignment
H_a	14	N−H···O−P	P_a	2	bound H_3PO_4
H_b	11−13	P−O−H···O−P	P_b	0.5	free H_3PO_4
H_c	10.5	free acid + ions	P_c	−10.5	bound $H_2PO_4^-$
H_d	5−9	aromatic	P_d	−12	free $H_2PO_4^-$

We have investigated four fuel cell samples, prepared as in Table 1. Line widths were measured and compared to conductivity measurements. The conductivity of the fuel cell membranes was calculated from the resistance of the cell:

$$\sigma = \frac{l}{(R_C - R_F)A} \tag{1}$$

where l is the membrane thickness, A is the membrane area, R_C is the resistance of the entire cell, and R_F is the resistance of the frame holding the membrane. In the measurements presented here, an assembly was used with $R_F = 6$ mΩ.

To gain an insight into the motional processes causing nuclear relaxation and conductivity, it is common to construct Arrhenius plots[5,12,13,28] of T_2* (the inverse of the full line width at half-height), and the conductivity, σ. The Arrhenius relation is suggested by a simple, two-site exchange model and takes the forms

$$T_2^* \propto \exp\left(-\frac{E_a^{(T_2^*)}}{RT}\right)$$
$$\sigma \propto \exp\left(-\frac{E_a^{(\sigma)}}{RT}\right) \tag{2}$$

for the two parameters under investigation. While such a model may be too simple for the system considered (deviations from linear behavior in such plots indicate non-Arrhenius behavior), the Arrhenius plots allow us to assess the temperature dependence of the parameters T_2* and σ. Figure 6 shows plots of ln T_2* and ln σ against 1000/T for the four fuel cell samples. Measurements of the gradients of these plots are given as activation energies in Table 3.

Of the three different T_2* values plotted in Figure 6, only H_d (on the polymer) has a linear dependence of ln T_2* upon T, indicating a steady increase in polymer mobility without a rubber/glass phase transition. The absence of such a transition in the temperature range studied is confirmed by a differential scanning calorimetry (DSC) study of PBI + H_3PO_4 (Figure 7), from which T_g is estimated to be 155 °C. Pronounced curvature is seen for the values of ln T_2* for the ^1H and ^{31}P nuclei in the acid, with the values passing through a maximum between 40 and 100 °C. This corresponds to a minimum in the line widths and implies that the local motion of the acid molecules is hindered at higher temperatures. The Arrhenius plots for the conductivities (Figure 6e−h) are also curved but do not pass through a maximum. Because the materials investigated are in the glass phase, this kind of behavior cannot be interpreted by the empirical Vogel−Tamman−Fulcher equation.[29]

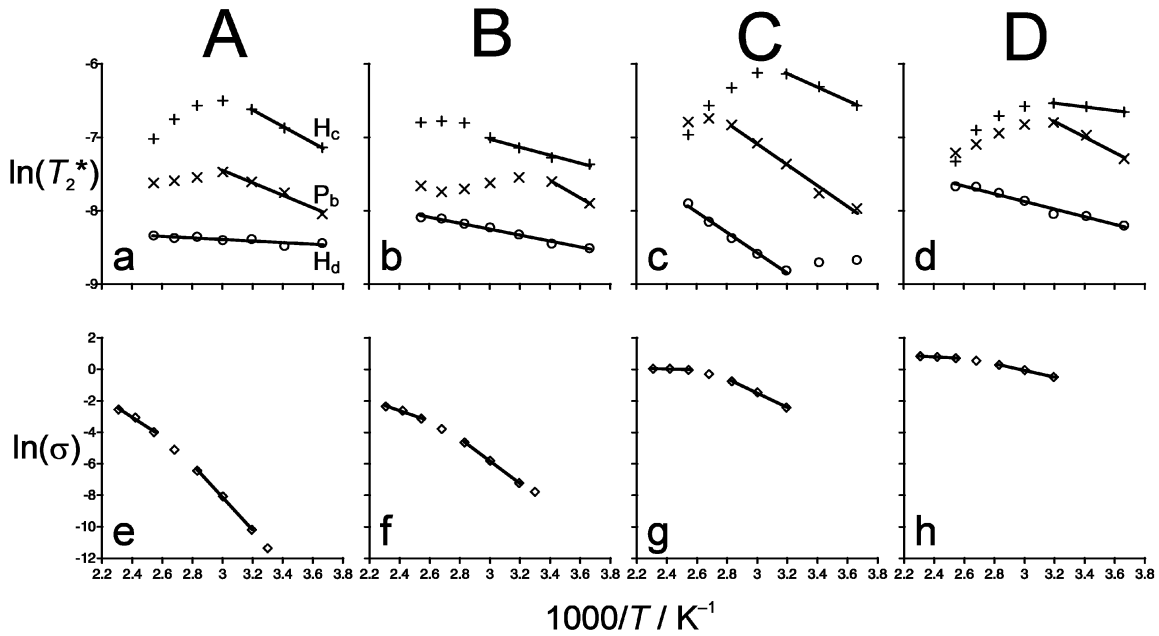

Figure 6. (a−d) Arrhenius plots of the ^{31}P transverse relaxation times (T_2*) for samples A−D, measured at 9.4 T and 6 kHz MAS. (×) ^{31}P resonance P_b; (+) ^{1}H resonance H_c; (○) ^{1}H resonance H_d. (e−h) Arrhenius plot of the conductivity (σ) of the same samples in fuel cells. Lines indicate regions for which gradients have been taken to calculate activation energies.

TABLE 3: Activation Energies[a] Calculated from Gradients of the Plots in Figure 6

	E_a from conductivity		E_a from nuclear relaxation		
sample	40 °C	160 °C	^{1}H (acid)	^{1}H (polymer)	^{31}P
A	86.2	51.4	7.80	1.25	4.47
B	59.3	27.6	9.83	3.36	5.36
C	38.0	2.60	11.8	11.53	7.66
D	17.8	4.53	8.82	4.32	2.11

[a] Activation energies, E_a, are given in kilojoules per mole.

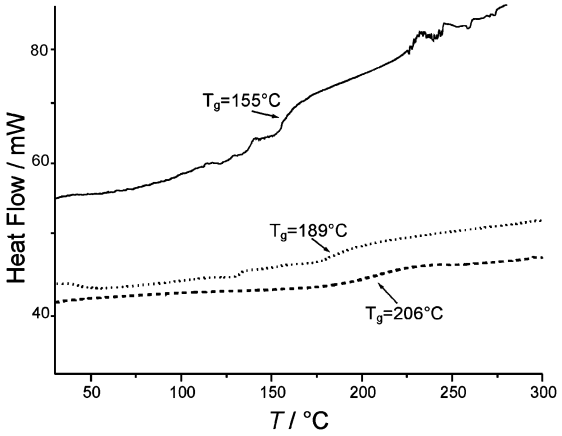

Figure 7. DSC measurements on PBI with three different H_3PO_4 doping levels: (—) 85 wt %, (•••) 68 wt %, and (---) 21 wt %. The glass transition temperature (T_g) is marked for each curve.

Higher doping or hydration levels generally increase the conductivity and reduce the corresponding activation energies (Table 3). For samples C and D (85 wt % doped) at high temperatures, activation energies are observed that are similar to that for proton mobility in water,[11,30] 10.9 kJ mol^{-1} (equivalent to the directional component of the H-bond enthalpy, associated with molecular rotation), while higher values are seen at lower temperatures for these samples and at all observed temperatures for samples A and B (70 wt % doped). However, no clear correlation between doping level or hydration and the nuclear relaxation times is seen, suggesting that little change occurs in the local mobility over the range of doping levels and hydration investigated. Notably, NMR spectra recorded at much lower doping levels exhibit significantly broader lines (shorter relaxation times), indicating that only at higher values does the doping level have little effect on the NMR spectra.

Conclusions

In the first part of our contribution, we have used two-dimensional SS NMR correlation methods and anisotropic chemical shift information to identify NMR signals resulting from local (i.e., dipolar through-space) acid−polymer interactions. We have observed protonation of the imidazole rings by the phosphoric acid (H_a), together with hydrogen bonding of both H_3PO_4 and $H_2PO_4^-$ to these sites (P_a and P_c). This implies that at least a part of the phosphoric acid cannot be involved in any bulk transport of protons. However, we have also found spectroscopic evidence for $H_2PO_4^-$ ions not bound to the polymer (P_d). Both the bulk transport and Grotthuss mechanisms would be expected to be accompanied by unbound $H_2PO_4^-$ ions, although only the bulk transport mechanism is entirely dependent upon their presence. In addition, hydrogen bonding between free H_3PO_4 has been observed (H_b). This would be a prerequisite for the Grotthuss mechanism but might be a hindrance to bulk transport.

The chemical shift assignments provide the spectroscopic basis for a study of the temperature-dependent dynamics of certain ^{1}H and ^{31}P resonances. These results were compared to conductivity measurements performed on PBI fuel cells. We have observed a reduction in local motion of the acid molecules and ions at higher temperatures. This reduction is not accompanied by a reduction in the conductivity but rather by a decline in the activation energy of conductivity. Had the two properties matched in their temperature dependence, this would have been a clear indication that small-scale motion, determinant for the NMR relaxation, was also determinant for the conductivity and that, hence, only the Grotthuss conduction mechanism was taking place. Instead, the data imply that larger-scale motions, not probed by MAS NMR, are also of significance for the conduction. Such motions may indicate either the

presence of some bulk transport or a Grotthuss-like mechanism, in which translation of the phosphoric acid accompanies the rearrangement of the hydrogen-bonding network.

Acknowledgment. This work was funded in part by an Alexander von Humboldt postdoctoral fellowship for C.E.H. and the Max-Planck-Gesellschaft.

References and Notes

(1) Wainright, J. S.; Wang, J.-T.; Weng, D.; Savinell, R. F.; Litt, M. *J. Electrochem. Soc.* **1995**, *142*, L121.
(2) Wang, J.-T.; Savinell, R. F.; Wainright, J.; Litt, M.; Yu, H. *Electrochim. Acta* **1996**, *41*, 193.
(3) Samms, S. R.; Wasmus, S.; Savinell, R. F. *J. Electrochem. Soc.* **1996**, *143*, 1225.
(4) Fontanella, J. J.; Wintersgill, M. C.; Wainright, J. S.; Savinell, R. F.; Litt, M. *Electrochim. Acta* **1998**, *43*, 1289.
(5) Bouchet, R.; Siebert, E. *Solid State Ionics* **1999**, *118*, 287.
(6) Glipa, X.; Bonnet, B.; Mula, B.; Jones, D. J.; Rozière, J. *J. Mater. Chem.* **1999**, *9*, 3045.
(7) Kawahara, M.; Morita, J.; Rikukawa, M.; Sanui, K.; Ogata, N. *Electrochim. Acta* **2000**, *45*, 1395.
(8) Li, Q.; Hjuler, H. A.; Bjerrum, N. J. *J. Appl. Electrochem.* **2001**, *31*, 773.
(9) Schuster, M. F. H.; Meyer, W. H. *Annu. Rev. Mater. Res.* **2003**, *33*, 233.
(10) Grotthuss, C. J. T. d. *Ann. Chim.* **1806**, *58*, 58.
(11) Agmon, N. *Chem. Phys. Lett.* **1995**, *244*, 456.
(12) Pu, H.; Meyer, W. H.; Wegner, G. *J. Polym. Sci., Polym. Phys.* **2002**, *40*, 663.
(13) Schechter, A.; Savinell, R. F. *Solid State Ionics* **2002**, *147*, 181.
(14) Bouchet, R.; Miller, S.; Duclot, M.; Souquet, J. L. *Solid State Ionics* **2001**, *145*, 69.
(15) Ma, Y.-L.; Wainright, J. S.; Litt, M. H.; Savinell, R. F. *J. Electrochem. Soc.* **2004**, *151*, A8.
(16) Schmidt-Rohr, K.; Spiess, H. W. *Multidimensional Solid-State NMR and Polymers*; Academic Press: San Diego, CA, 1994.
(17) Andrew, E. R.; Bradbury, A.; Eades, R. G. *Nature* **1958**, *182*, 1659.
(18) Brown, S. P.; Spiess, H. W. *Chem. Rev.* **2001**, *101*, 4125.
(19) Hronska, M.; van Beek, J. D.; Williamson, P. T. F.; Vollrath, F.; Meier, B. H. *Biomacromolecules* **2004**, *5*, 834.
(20) Luca, S.; Heise, H.; Baldus, M. *Acc. Chem. Res.* **2003**, *36*, 858.
(21) Kim, N.; Grey, C. P. *Science* **2002**, *297*, 1317.
(22) Sartorius AG, Patent DE 101 55 543 C2.
(23) *Gmelins Handbuch Der Anorganischen Chemie*; Kotowski, A., Ed.; Verlag: Weinheim, Germany, 1965; Vol. Phosphor Teil C, p 169.
(24) Hartmann, S. R.; Hahn, E. L. *Phys. Rev.* **1962**, *128*, 2042.
(25) Metz, G.; Wu, X. L.; Smith, S. O. *J. Magn. Reson. A* **1994**, *110*, 219.
(26) Caravatti, P.; Braunschweiler, L.; Ernst, R. R. *Chem. Phys. Lett.* **1983**, *100*, 305.
(27) Ernst, R. R.; Bodenhausen, G.; Wokaun, A. *Principles of Nuclear Magnetic Resonance in One and Two Dimensions*; Clarendon Press: Oxford, U.K., 1987.
(28) Goward, G. R.; Schuster, M. F. H.; Sebastiani, D.; Schnell, I.; Spiess, H. W. *J. Phys. Chem. B* **2002**, *106*, 9322.
(29) *Proton Conductors: Solids, Membranes and Gels—Materials and Devices*; Colomban, P., Ed.; Cambridge University Press: Cambridge, U.K., 1992.
(30) Kreuer, K. D. *Solid State Ionics* **2000**, *136−137*, 149.